NACA

RESEARCH MEMORANDUM

ROCKET-MODEL INVESTIGATION OF LONGITUDINAL STABILITY AND

DRAG CHARACTERISTICS OF AN AIRPLANE CONFIGURATION

HAVING A 60° DELTA WING AND A HIGH

UNSWEPT HORIZONTAL TAIL

By Robert F. Peck and Jesse L. Mitchell

Langley Aeronautical Laboratory
Langley Field, Va.

RECEIPT SIGNATURE
REQUIRED

NATIONAL ADVISORY COMMITTEE
FOR AERONAUTICS
WASHINGTON
January 5, 1953

NATIONAL ADVISORY COMMITTEE FOR AERONAUTICS

RESEARCH MEMORANDUM

ROCKET-MODEL INVESTIGATION OF LONGITUDINAL STABILITY AND

DRAG CHARACTERISTICS OF AN AIRPLANE CONFIGURATION

HAVING A 60° DELTA WING AND A HIGH

UNSWEPT HORIZONTAL TAIL

By Robert F. Peck and Jesse L. Mitchell

SUMMARY

    A rocket-propelled model of an airplane configuration having a
60° delta wing with an NACA 65A003 airfoil section and a high unswept
horizontal tail has been flown by the Langley Pilotless Aircraft Research
Division. The results obtained at Mach numbers between 0.9 and 1.37
indicate little variation in lift-curve slope and in static and dynamic
stability with change in Mach number and no abrupt trim changes. Sta-
bility parameters and lift-curve slope show effects of varying lift,
however, which might be explained by the horizontal tail being in a posi-
tion where the downwash variation with angle of attack increased with
lift. At a Mach number of approximately 0.90, the model was pitched to
angles of attack above 20°. This probably resulted from reduced stabil-
ity, at the higher lift coefficients, stemming from the high tail loca-
tion. The exposed wing lift-curve slope showed little variation with
lift and agrees satisfactorily at supersonic speeds with values calculated
by an approximate linearized theory.

INTRODUCTION

    The longitudinal stability, lift, and drag characteristics of air-
plane configurations at transonic and supersonic speeds are being inves-
tigated by the NACA using rocket-propelled models in free flight. The
effects of variations in wing geometry on the longitudinal aerodynamic
characteristics are being investigated in a correlated program in which
various wings are test-flown on a basic fuselage-empennage arrangement
(refs. 1 to 5). The data from these models are obtained from telemetered
records of the response of the models to a square-wave variation of
horizontal-tail incidence.

The purpose of the present paper is to present the results obtained from the flight of one of the general research test vehicles which had a $60°$ delta wing with an NACA 65A003 airfoil section. Data presented include lift, drag, pitching moment, and damping in pitch of the complete configuration in addition to exposed wing lift. The Mach number range covered by the test is from 0.9 to 1.37 and Reynolds number from 8.4×10^6 to 13.8×10^6.

The tests were made at the Langley Pilotless Aircraft Research Station at Wallops Island, Va.

SYMBOLS

C_N	normal-force coefficient, $\dfrac{a_n}{g} \dfrac{W/S}{q}$
C_{N_e}	normal-force coefficient of exposed wing based on total wing area, N_e/qS
C_c	chord-force coefficient, $\dfrac{-a_l}{g} \dfrac{W/S}{q}$
C_L	lift coefficient, $C_N \cos \alpha - C_c \sin \alpha$
C_D	drag coefficient, $C_c \cos \alpha + C_N \sin \alpha$
a_n/g	normal accelerometer reading
a_l/g	longitudinal accelerometer reading
N_e	corrected wing balance reading, lb
g	acceleration due to gravity, ft/sec^2
α	angle of attack, deg
W	weight of model, lb
S	wing area (including area inclosed within fuselage) sq ft
S_e	exposed wing area, sq ft
q	dynamic pressure, lb/sq ft
C_m	pitching-moment coefficient

θ angle of pitch, radians

$\ddot{\theta}$ angular acceleration in pitch, radians/sec^2

$\overline{c}$ wing mean aerodynamic chord, ft

I   moment of inertia in pitch, slug-ft^2

l distance between nose and center-of-gravity normal
          accelerometers, ft

δ horizontal-tail deflection, deg

M   Mach number

V   velocity, ft/sec

R   Reynolds number based on mean aerodynamic chord

P   period of oscillation, sec

$T_{1/2}$ time to damp to one-half amplitude, sec

t   time

Subscripts:

$$\dot{\alpha} = \frac{1}{57.3} \frac{d\alpha}{dt} \frac{\overline{c}}{2V}$$

$$q = \frac{d\theta}{dt} \frac{\overline{c}}{2V}$$

e   exposed

WF   wing fuselage

cg   center of gravity

The symbols α, q, and $\dot{\alpha}$ used as subscripts indicate the derivative of the quantity with respect to the subscript.

MODELS AND APPARATUS

Model

A sketch of the configuration used in this investigation is shown in figure 1. A 60° delta wing with an NACA 65A003 airfoil section was mounted on a basic fuselage-empennage arrangement similar to that used in references 1 to 5. Fuselage ordinates are given in reference 3. The lower vertical fin was installed on the model to minimize roll or yaw motions which might perniciously influence the longitudinal maneuver in a manner noted in reference 5.

The wing was constructed of solid steel; the horizontal tail, of solid duralumin; the fuselage, of magnesium and steel; and the vertical tails, of wood with duralumin skin.

The incidence of the horizontal tail was varied in an approximate square-wave pattern by means of a hydraulic pulsing system. The tail settings used were -1.16° and -5.43° (with respect to the wing).

The model weight was 142.3 pounds, the center of gravity was at 20.6 percent of the mean aerodynamic chord, and the moment of inertia in pitch was 11.56 slug-ft^2.

Instrumentation

The model was equipped with a 10-channel telemeter transmitting continuous measurements of normal acceleration near the center of gravity and at a point about 3 feet ahead of the center of gravity, longitudinal and transverse accelerations, angle of attack, horizontal-tail position, two measurements of exposed wing normal force, total pressure, and a reference static pressure.

A vane-type angle-of-attack indicator which had a range of 15° to -10° relative to the sting was mounted on a bent sting so as to provide angle-of-attack instrument range up to approximately +21°.

Wing normal force was measured by means of a beam-type wing balance equipped with an inductance-type pickup. Gaps at the wing-fuselage juncture were sealed with fabric. A strain gage was attached to the wing balance primarily to gain experience in telemetering strain-gage measurements. The wing-normal-force data presented herein were obtained from the inductance pickup record.

The total-pressure tube was mounted on a strut below the fuselage as shown in figure 1. A static-pressure orifice was located on the top

of the fuselage 0.70 body diameter behind the forward station of the
cylindrical portion of the fuselage.

SCR 584 radar was used to determine the flight path of the model
as a function of time. Atmospheric conditions at the time of the flight
were determined from radiosonde data.

Mach number of the model was obtained from the telemetered total
pressure measurements and the static pressures obtained from the SCR 584
radar and radiosonde data.

TESTS AND ANALYSIS

The model was launched at a 60° elevation angle from a mobile
launching platform (fig. 2). A 6-inch-diameter solid-fuel ABL Deacon
rocket motor was used to boost the model to a Mach number of 1.39. The
model, which had no sustainer rocket, separated from the booster at
rocket burnout by virtue of its lower drag-weight ratio. The data were
obtained during the decelerating portion of the flight as the model
responded in pitch to the square-wave variation of horizontal-tail
incidence in a manner indicated by the portion of telemeter record shown
in figure 3. There were no appreciable transverse accelerations during
the portion of flight over which data were obtained.

The short-period-pitch oscillations resulting from the deflection
of the horizontal tail were analyzed by the methods of appendix A, refer-
ence 1, to determine the trim, longitudinal stability, lift, and drag
characteristics of the model. In addition, the data from the two normal
accelerometers were used to obtain total pitching-moment data as follows:

The pitching acceleration $\ddot{\theta}$ is given by

$$\ddot{\theta} = \frac{g}{l}\left[(a_n/g)_{nose} - (a_n/g)_{cg}\right]$$

which is proportional to total-pitching-moment coefficient

$$C_{m_{total}} = \frac{I}{qS\bar{c}}\ddot{\theta}$$

The Reynolds number of the test varied with Mach number as indicated
in figure 4.

CORRECTIONS AND ACCURACY

Corrections

The wing normal forces obtained from the wing balance included not only aerodynamic normal forces but also inertial forces exerted by the wing and the moving parts of the wing balance. The total normal forces read by the balance were corrected for these inertial forces through use of normal-acceleration data and the weights of the contributing components. The aerodynamic normal force was converted to coefficient form and the exposed wing lift coefficient was assumed given by $C_{L_e} = C_{N_e} \cos \alpha$.

The angle of attack at the center of gravity was obtained from the angle-of-attack measurements made at the nose of the model by the method outlined in reference 6.

By use of the $C_{m_q} + C_{m_{\dot\alpha}}$ data obtained from this test and the assumption that the value of C_{m_q} was primarily that contributed by the horizontal tail, the relatively small pitching moments due to damping were estimated and subtracted from the total pitching moment, as obtained by the method briefly described in the foregoing section, to obtain pitching moment due to angle of attack.

Accuracy

Possible systematic errors in the absolute values of directly measured quantities are proportional to the total range of the instrumentation involved. Possible errors obtained by assuming an accuracy of approximately ±1 percent of the total instrument range are presented in the following table:

M	ΔC_N	ΔC_C	ΔC_{N_e}	$\Delta \delta$	$\Delta \alpha$
1.35	±0.01	±0.002	±0.01	±0.04	±0.25
.9	±.02	±.004	±.015	±.04	±.25

Experience has shown the accuracy of variations in the various quantities far exceeds the accuracy of the absolute values indicated by the foregoing table. This is verified by the relatively small amount of scatter of individual points in the basic data plots shown herein. The Mach number is believed accurate within ±0.01 throughout the test.

The angle-of-attack indicator may be subject to a further possible error in absolute angle of attack of ±0.5° due to small asymmetries in the vane which may cause it to float at small angles relative to the air stream.

In this particular investigation, at Mach numbers below 1.15, the angle-of-attack measurements were subject to further error as evidenced by recorded flat peaks on the angle-of-attack oscillations. These flat peaks and a lag in angle-of-attack readings are believed due to excessive friction in the indicator which was greatly reduced at the higher Mach numbers by shaking of the nose section. This is illustrated in figure 3 where the portions of telemeter record taken just before and after the nose shaking ceased are shown.

RESULTS AND DISCUSSION

Trim

The trim lift and angle-of-attack characteristics for the two tail deflections used are shown in figure 5. The solid portions of the lines indicate regions where trim was actually measured as the mean line of the pitch oscillation. No abrupt trim changes are indicated in the Mach number range covered.

Lift

Plots of variation of lift (both total and exposed wing) with angle of attack during the first one and one-half cycles of the pitch oscillations are presented in figure 6. The Mach number change occurring during the one and one-half cycles shown was the order of 0.04 for the high lift and about 0.02 for the low lift oscillations. The Mach numbers quoted in the figure were the average during the portions of oscillations presented.

The difference between C_L obtained under conditions of α increasing with time and those with α decreasing with time results, it is believed, primarily from an α lag effect caused by excessive friction in the angle-of-attack indicator as discussed briefly in the section entitled "Accuracy." The slopes do not appear to be appreciably affected by the sign of $d\alpha/dt$ except at the peaks of the oscillations.

The lift-curve plots for a Mach number of 0.90 indicate a lift break at an angle of attack of about 14.5°. This lift break was apparently associated with the wing since it was indicated by the wing balance record as well as by the normal accelerometers. A similar but less

abrupt break in lift curve is indicated by wind-tunnel data on a delta
wing of aspect ratio 2 (ref. 7). Differences in indicated abruptness
of the lift break are probably due to the comparatively low number of
wind-tunnel test points in the lift-break range.

The model pitched beyond the lift break to angles of attack exceeding
the range of the angle-of-attack indicator and, during the time it was
at these high angles, the Mach number dropped to values too low to be
measured accurately by the instrumentation used. As the angle-of-attack
instrument limits were approached, a combined pitch-lateral maneuver
occurred as indicated by relatively high values of lateral acceleration;
therefore no data were obtained below a Mach number of 0.90 where the
lift break and pitch-up occurred.

Lift-curve slopes were measured about the trim value of C_L and α.
Variations of lift-curve slope with Mach number as obtained for the total
model and for the exposed wing are given in figures 7(a) and 7(b),
respectively.

Lift-curve slope of the total configuration (fig. 7(a)) at the high
lifts is indicated to be somewhat lower than that at the lower lifts.
It is believed that this primarily resulted from the horizontal tail
being in a position such that the downwash variation with angle of attack
$d\epsilon/d\alpha$ was greater as the lift increased. This type variation of $d\epsilon/d\alpha$
with C_L is indicated by data in references 8 and 9. The exposed wing-
lift-curve slope (fig. 7(b)) indicated only a small amount of nonlinearity
over the lift range covered, which supports the foregoing statement con-
cerning the downwash variation.

Results of previous work such as those given in reference 10 have
shown that exposed wing-lift-curve slope may be estimated in many cases
by multiplying the lift-curve slope of the wing fuselage by the ratio
of exposed to total wing area. The lift-curve slope of the wing fuselage
used in the present test was obtained by subtracting the lift-curve slope
of the tail from the lift-curve slope of the total configuration at the
low lifts. The lift-curve slope of the tail was obtained from data of
reference 2 and downwash values based on data of references 9 and 11. It
can be seen from figure 7(b) that, in this particular instance, using
the area ratio to approximate wing-lift-curve slope results in values
appreciably lower than those measured. This indicates that this estimate
is not applicable to configurations with comparatively low values of S_e/S.
A closer estimate of the exposed wing-lift-curve slope may be obtained
for supersonic speeds from the approximate linearized theory of
reference 12.

There was no definite indication of wing buffeting except near a
Mach number of 0.90 at lift coefficients at and above the lift break

where a relatively mild but irregular shaking was experienced. The vibration of the nose which occurred above Mach numbers of about 1.15 (fig. 3(a)) is not attributed to wing buffeting. The frequency of this shaking corresponds to a body-nose bending frequency determined by shake tests made before the flight and the occurrence of such a vibration has been noted in the same Mach number region on another model with the same fuselage-empennage but a different wing plan form (unpublished data).

Drag

The basic drag data are presented in the form of polars in figure 8. The effect of varying Mach number on drag coefficient in the drag-break region is evident in the variation of points in the polar for an average Mach number of 0.99. Variation of drag coefficient with Mach number at several constant lift coefficients and the two tail settings is given in figure 9. The increase in drag coefficient as the Mach number increased from 1.2 to 1.35 is contrary to the trends indicated by data of reference 5. The reasons for this increase are not known but may be due to effects of interference or to the nose shaking shown in figure 3 which was evidenced at Mach numbers above 1.15. A large portion of the change in drag coefficient resulting from a change in tail incidence is the change in the streamwise component of the tail normal-force coefficient with change in tail incidence.

Variations of the induced drag factors $\dfrac{dC_D}{dC_L{}^2}$ and $\dfrac{1}{57.3C_{L_\alpha}}$ with Mach number are presented in figure 10. The data indicate that, at low lift coefficients ($\delta = -1.16$), the resultant force vector due to angle of attack was tilted forward. However, at the higher lift coefficients the vector was essentially normal to the wing as indicated by coincidence of $\dfrac{dC_D}{dC_L{}^2}$ and $\dfrac{1}{57.3C_{L_\alpha}}$. This effect is in agreement with data presented in reference 13.

Static Stability

The variation of pitching-moment coefficient with lift coefficient is shown in figure 11. The values of C_m presented in this figure were obtained from two normal accelerometers by methods discussed in foregoing sections of this paper. The variations of period of the pitch oscillations and the stability parameters C_{m_α} and dC_m/dC_L with Mach number are shown in figure 12. Values of dC_m/dC_L shown in figure 12(c) were obtained from the data of figure 11 and also from C_{m_α} in figure 12(b)

divided by C_{L_α} shown in figure 7. Agreement of dC_m/dC_L values determined from these two methods is good.

The fairly smooth variation of static stability with Mach number was similar to variations obtained from somewhat similar delta-wing configurations reported in references 5 and 13. The stability decreased with increase in lift coefficient. This decrease is evident in figure 11 at Mach numbers of 0.99 and 0.90. At a Mach number of 0.90 the data were obtained almost to a lift coefficient of 1.0 and indicate a very severe loss of stability and a pitch-up at lift coefficients above 0.75 which, is the point where the sharp break in lift occurred.

It is believed that the primary factor contributing to the decrease in stability with increase in lift, at lift coefficients below the lift break, was an increase in $d\epsilon/d\alpha$ at the tail with an increase in lift. This was associated with the high tail position and was mentioned in the section entitled "Lift" of this report as a possible cause of the reduction in total-lift-curve slope with increase in lift coefficient.

Damping in Pitch

Figure 13 presents the information obtained on the damping characteristics of the pitch oscillations resulting from the abrupt control movements. Figure 13(a) shows the amplitude ratio measured from the trim line as a function of time. The data have been faired by a straight line on the semilog plots. The time for the oscillations to damp to one-half amplitude as determined from the faired curves is shown in figure 13(b). These times to damp, along with the lift-curve slopes from figure 7, have been used to determine the rotary-damping parameter $C_{m_q} + C_{m_{\dot\alpha}}$ (fig. 13(c)). An increase in $C_{m_q} + C_{m_{\dot\alpha}}$ with increase in lift coefficient is indicated. An increase in $d\epsilon/d\alpha$ with increase in lift coefficient mentioned in the "Lift" and "Static Stability" sections of this report could account for this increase in $C_{m_q} + C_{m_{\dot\alpha}}$ through its effect in increasing $C_{m_{\dot\alpha}}$.

Comparisons

Comparisons are made in figure 14 between data from the present test and data from references 2, 5, and 13. Reference 2 contains data on the wingless fuselage empennage used on the model of the present test. The longitudinal characteristics of an airplane configuration with the same fuselage-empennage group without lower vertical tail and with a modified delta wing are presented in reference 5 and the longitudinal characteristics of a tailless configuration with a 60° delta wing having an NACA $65_{(06)}A006.5$ airfoil section are presented in reference 13. For

purposes of comparison, the drag of one vertical tail, obtained from reference 2, was added to the drag of the model of reference 5.

In general, the parameters compared show the same variation with Mach number, and differences in level may be explained by differences in configurations. The model of reference 13 had no horizontal tail and therefore would be expected to differ from the models of the present test and reference 5 as indicated. The small differences in lift-curve slope, aerodynamic center, and induced drag between the models of the present test and reference 5 are compatible with the slightly higher aspect ratio of the model of reference 5. However, the differences in supersonic minimum drag of these two models are contrary to what might be expected. These differences are in general of the same order as the accuracy of the drag data; however, the drag of the present model may have been increased by unfavorable interference of the lower vertical tail or by nose shaking (at the higher Mach numbers) as discussed briefly in the "Drag" section of the present report.

CONCLUSIONS

A rocket-propelled model has been flown to determine the longitudinal stability and drag characteristics of an airplane configuration with a 60° delta wing with an NACA 65A003 section and a high unswept horizontal tail. The data indicate the following:

1. The variations of lift-curve slope, static stability, and pitch-damping parameter $\left(C_{m_q} + C_{m_{\dot{\alpha}}}\right)$ with Mach number were smooth and relatively small and no abrupt trim changes were encountered.

2. Total-lift-curve slope and static stability decreased and the pitch-damping parameter $\left(C_{m_q} + C_{m_{\dot{\alpha}}}\right)$ increased with increasing lift coefficient, all of which could be accounted for by the horizontal tail being in a position where there was an increase in rate of change of downwash with angle of attack as the lift coefficient increased.

3. The exposed wing-lift-curve slope showed only a small variation with change in lift coefficient, agrees satisfactorily at supersonic speeds with values calculated by an approximate linearized theory, but is appreciably higher than values estimated by multiplying lift-curve slope of the wing fuselage by the ratio of the exposed to total wing area.

4. At a Mach number of approximately 0.90, the reduced stability at the higher lift coefficients, stemming primarily from a high tail location, resulted in the model pitching up to angles of attack above 20°.

An abrupt break in lift was indicated both by the total lift and wing
lift measurements at a total lift coefficient of approximately 0.75.

  5. In general, data obtained at low lift show the same effects of
Mach number variation as comparable data from other delta-wing tests.

Langley Aeronautical Laboratory,
     National Advisory Committee for Aeronautics,
          Langley Field, Va.

REFERENCES

1. Gillis, Clarence L., Peck, Robert F., and Vitale, A. James: Pre-
liminary Results From a Free-Flight Investigation at Transonic and
Supersonic Speeds of the Longitudinal Stability and Control Charac-
teristics of an Airplane Configuration With a Thin Straight Wing of
Aspect Ratio 3. NACA RM L9K25a, 1950.

2. Gillis, Clarence L., Vitale, A. James: Wing-on and Wing-Off Longi-
tudinal Characteristics of an Airplane Configuration Having a Thin
Unswept Tapered Wing of Aspect Ratio 3, As Obtained From Rocket-
Propelled Models at Mach Numbers From 0.8 to 1.4. NACA RM L50K16,
1951.

3. Vitale, A. James, McFall, John C., Jr., and Morrow, John D.:
Longitudinal Stability and Drag Characteristics at Mach Numbers
From 0.75 to 1.5 of an Airplane Configuration Having a 60° Swept
Wing of Aspect Ratio 2.24 As Obtained From Rocket-propelled Models.
NACA RM L51K06, 1952.

4. Parks, James H.: Longitudinal Aerodynamic Characteristics of a Model
Airplane Configuration Equipped With a Scaled X-1 Airplane Wing.
NACA RM L51L10a, 1952.

5. Chapman, Rowe, Jr., and Morrow, John D.: Longitudinal Stability and
Drag Characteristics at Mach Numbers From 0.70 to 1.37 of Rocket-
Propelled Models Having a Modified Triangular Wing. NACA
RM L52A31, 1952.

6. Mitchell, Jesse L., and Peck, Robert F.: An NACA Vane-Type Angle-
of-Attack Indicator for Use at Subsonic and Supersonic Speeds. NACA
RM L9F28a, 1949.

7. Smith, Donald W., and Heitmeyer, John C.: Lift, Drag, and Pitching
Moment of Low-Aspect-Ratio Wings at Subsonic and Supersonic Speeds -
Plane Triangular Wing of Aspect Ratio 2 With NACA 0005-63 Section.
NACA RM A50K21, 1951.

8. Mitchell, Jesse L.: The Static and Dynamic Longitudinal Stability
Characteristics of Some Supersonic Aircraft Configurations. NACA
RM L52A10a, 1952.

9. Allen, Edwin C.: Investigation of a Triangular Wing in Conjunction
With a Fuselage and Horizontal Tail To Determine Downwash and
Longitudinal-Stability Characteristics - Transonic Bump Method.
NACA RM A51F12a, 1951.

10. Mayer, John P., and Gillis, Clarence L.: Division of Load Among the Wing, Fuselage, and Tail of Aircraft. NACA RM L51E14a, 1951.

11. Graham, David, and Koenig, David G.: Tests in the Ames 40- by 80-Foot Wing Tunnel of an Airplane Configuration With an Aspect Ratio 2 Triangular Wing and an All-Movable Horizontal Tail - Longitudinal Characteristics. NACA RM A51B21, 1951.

12. Tucker, Warren A.: A Method for Estimating the Components of Lift of Wing-Body Combinations at Supersonic Speeds. NACA RM L52D22, 1952.

13. Mitcham, Grady L., Crabill, Norman L., and Stevens, Joseph E.: Flight Determination of the Drag and Longitudinal Stability and Control Characteristics of a Rocket-Powered Model of a 60° Delta-Wing Airplane From Mach Numbers of 0.75 to 1.70. NACA RM L51I04, 1951.
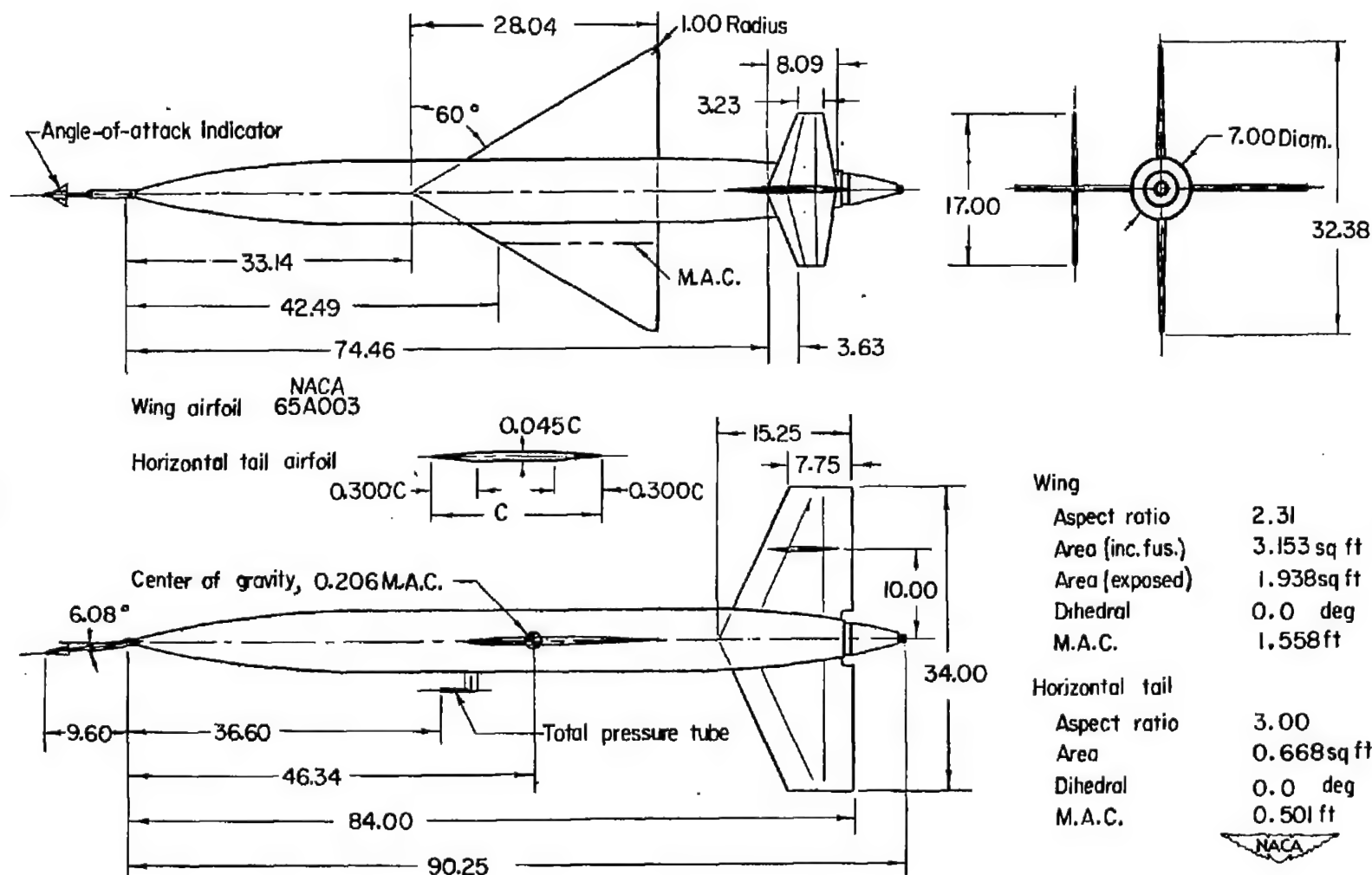
Figure 1.- General arrangement of the model. All dimensions are in inches.

28.04

1.00 Radius

8.09

3.23

60°

Angle-of-attack Indicator

7.00 Diam.

17.00

32.38

33.14

42.49

M.A.C.

74.46

3.63

NACA
Wing airfoil   65A003

Horizontal tail airfoil

0.045C

0.300C

0.300C

C

15.25

7.75

Center of gravity, 0.206 M.A.C.

10.00

6.08°

34.00

9.60

36.60

Total pressure tube

46.34

84.00

90.25

Wing
   Aspect ratio   2.31
   Area (inc. fus.)   3.153 sq ft
   Area (exposed)   1.938 sq ft
   Dihedral   0.0 deg
   M.A.C.   1.558 ft

Horizontal tail
   Aspect ratio   3.00
   Area   0.668 sq ft
   Dihedral   0.0 deg
   M.A.C.   0.501 ft

Figure 2.- Photograph of model and booster on launcher.

L-73772.1
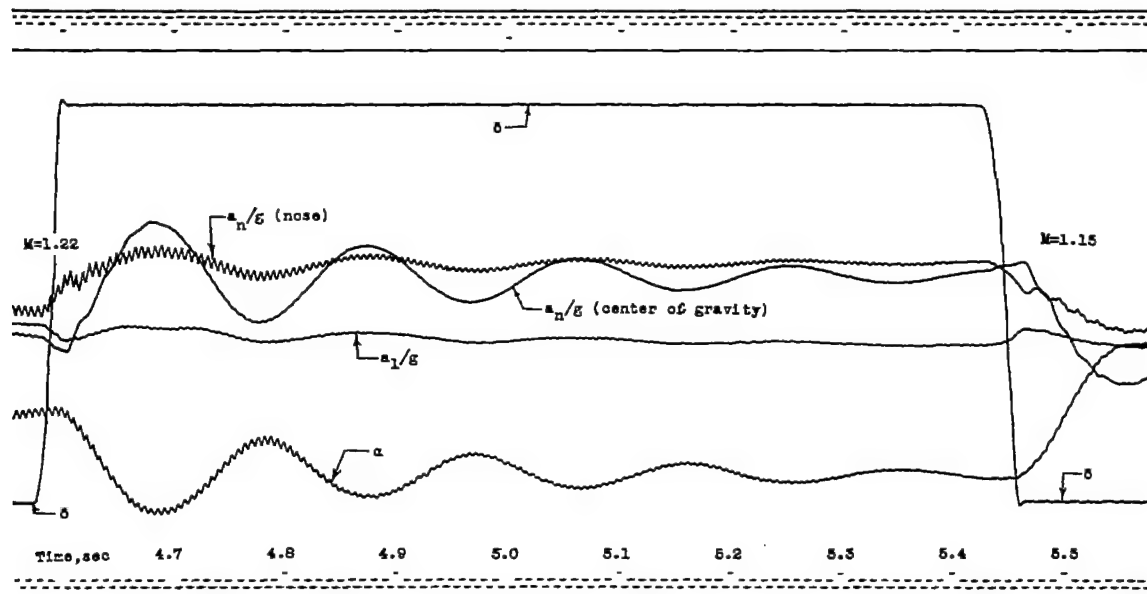
(a) During nose shaking.
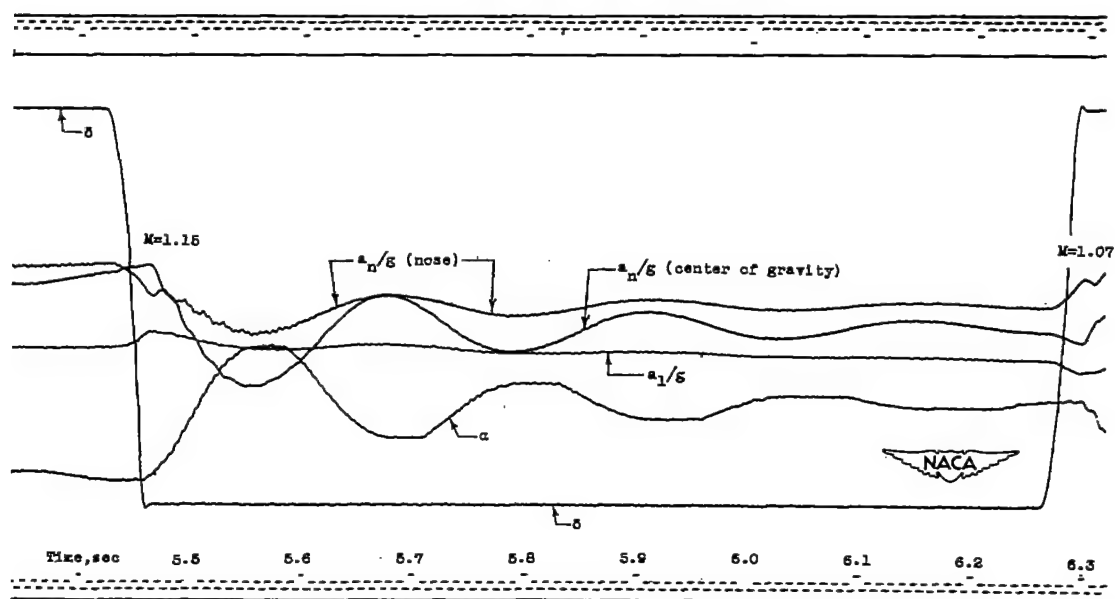
(b) After shaking ceased.

Figure 3.- Portion of telemeter record taken during and after nose shaking.
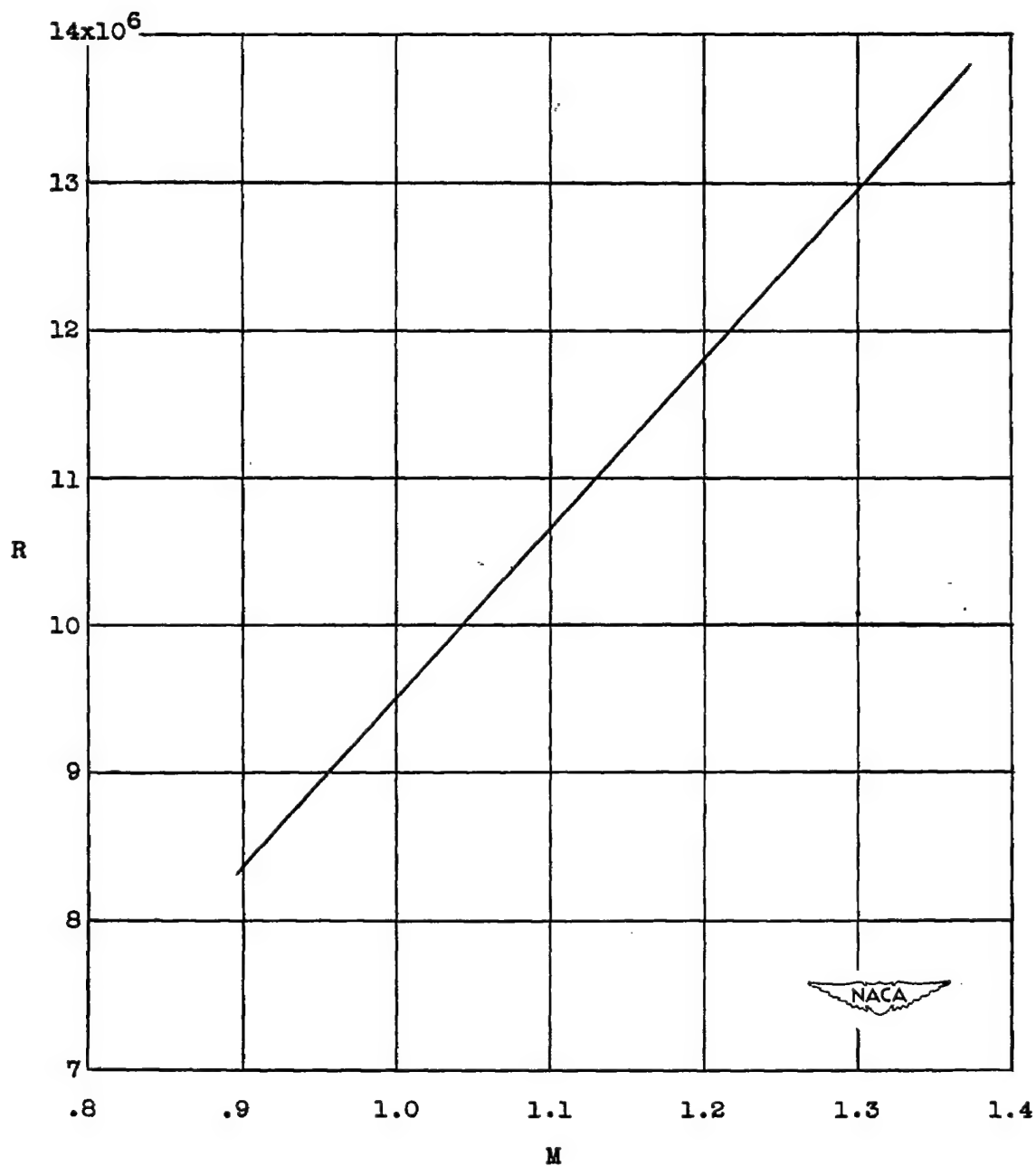
Figure 4.- Test Reynolds number based on mean aerodynamic chord.
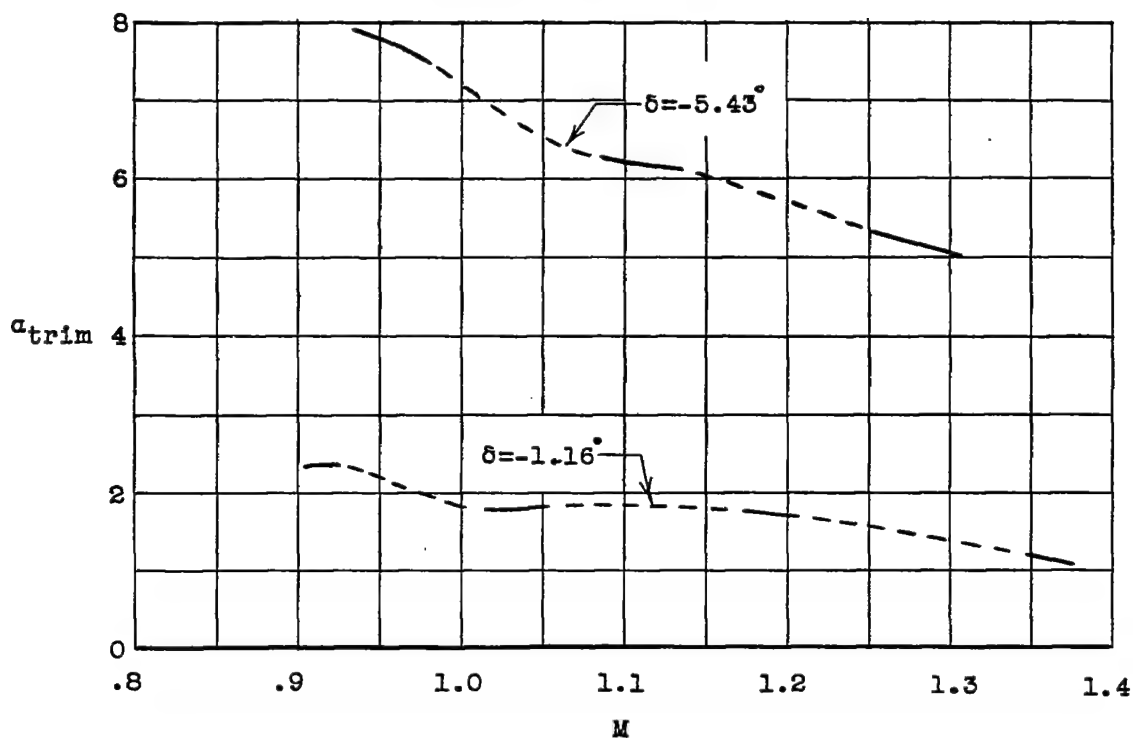
(a)   Trim angle of attack.
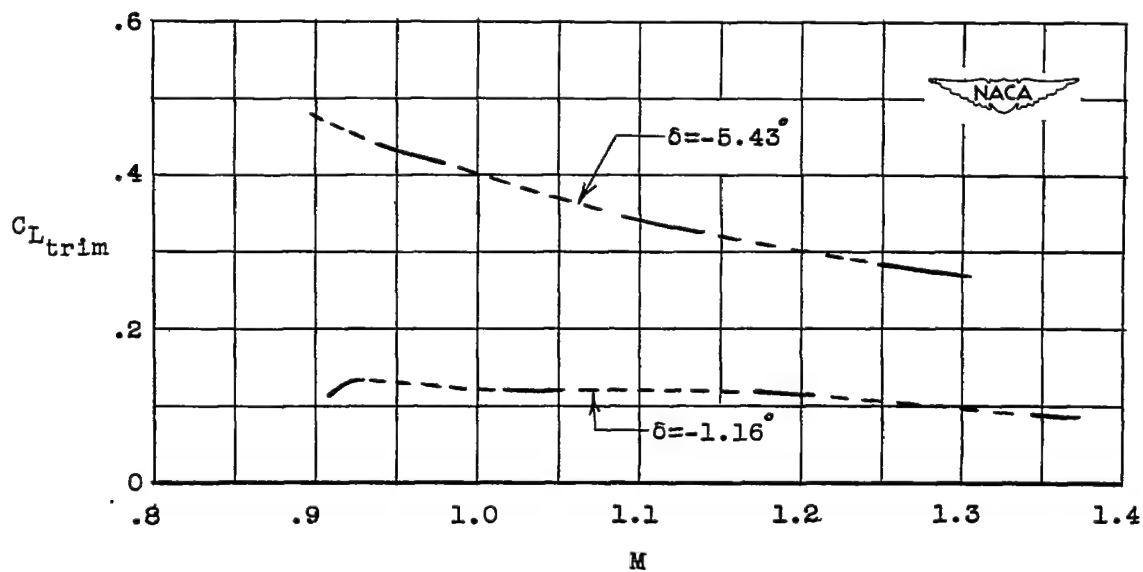
(b)   Trim lift.

Figure 5.- Trim lift and angle-of-attack characteristics.
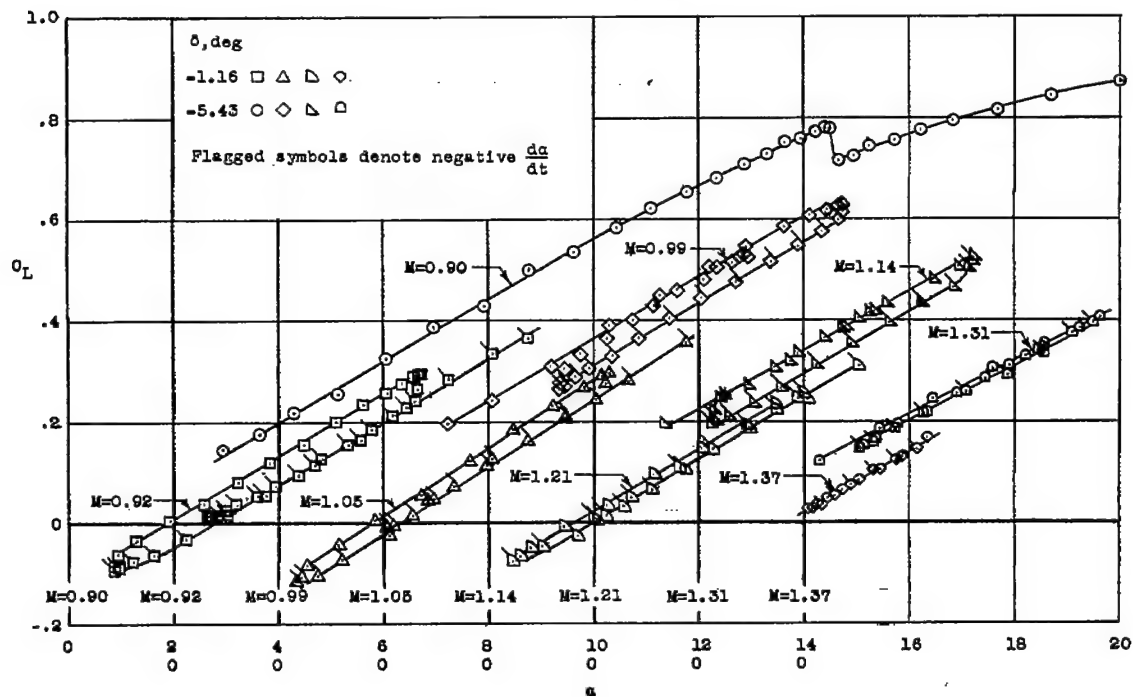
(a) Total configuration.
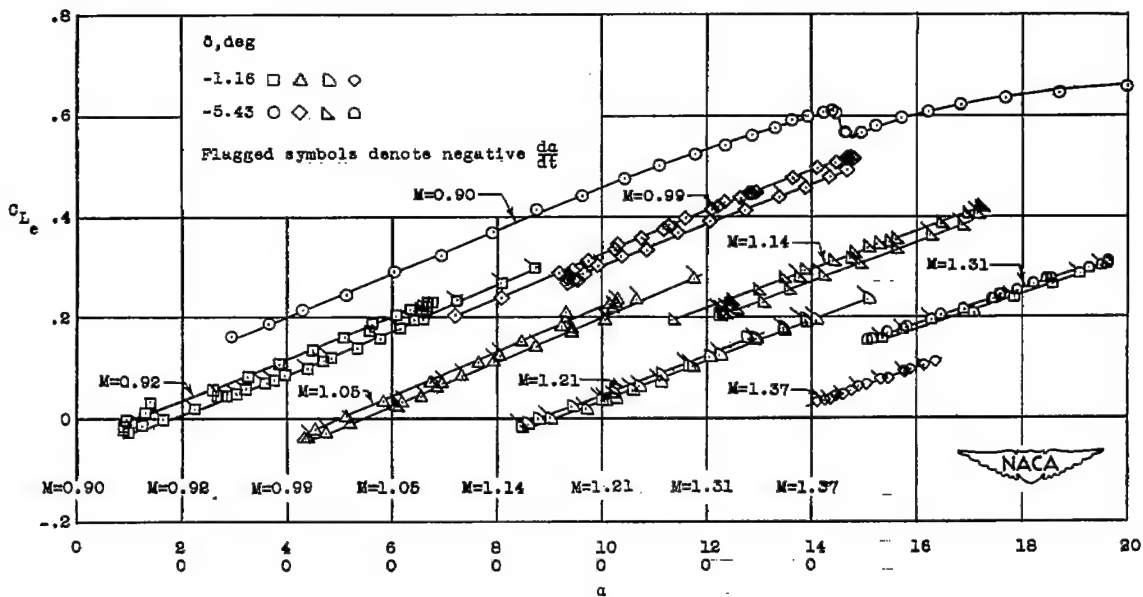
(b) Exposed wing.

Figure 6.- Variation of lift coefficient with angle of attack.

$\delta=-1.16°$

$\delta=-5.43°$

(a) Total configuration.

$\delta=-5.43°$ $\delta=-1.16°$

$(S_e/S)C_{L_{\alpha_{WF}}}$ Theory (reference 12)
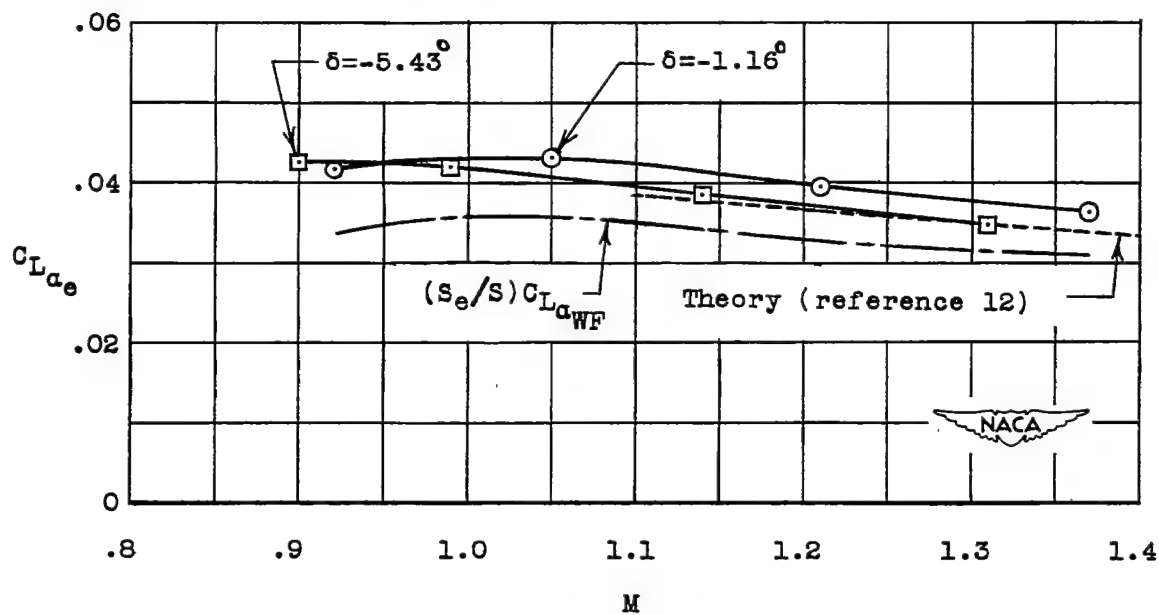
(b) Exposed wing.

Figure 7.- Lift-curve slope.
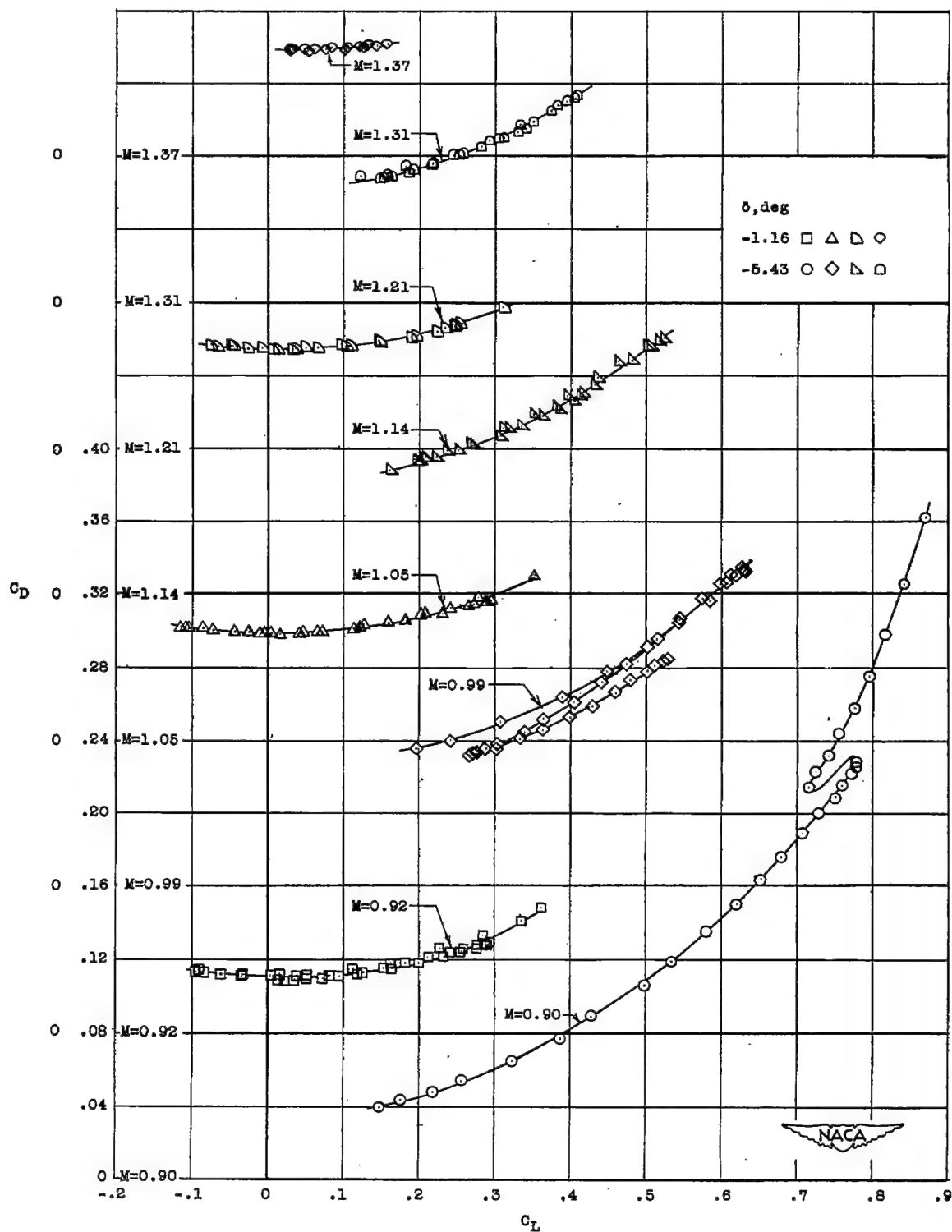
Figure 8.- Drag polars.
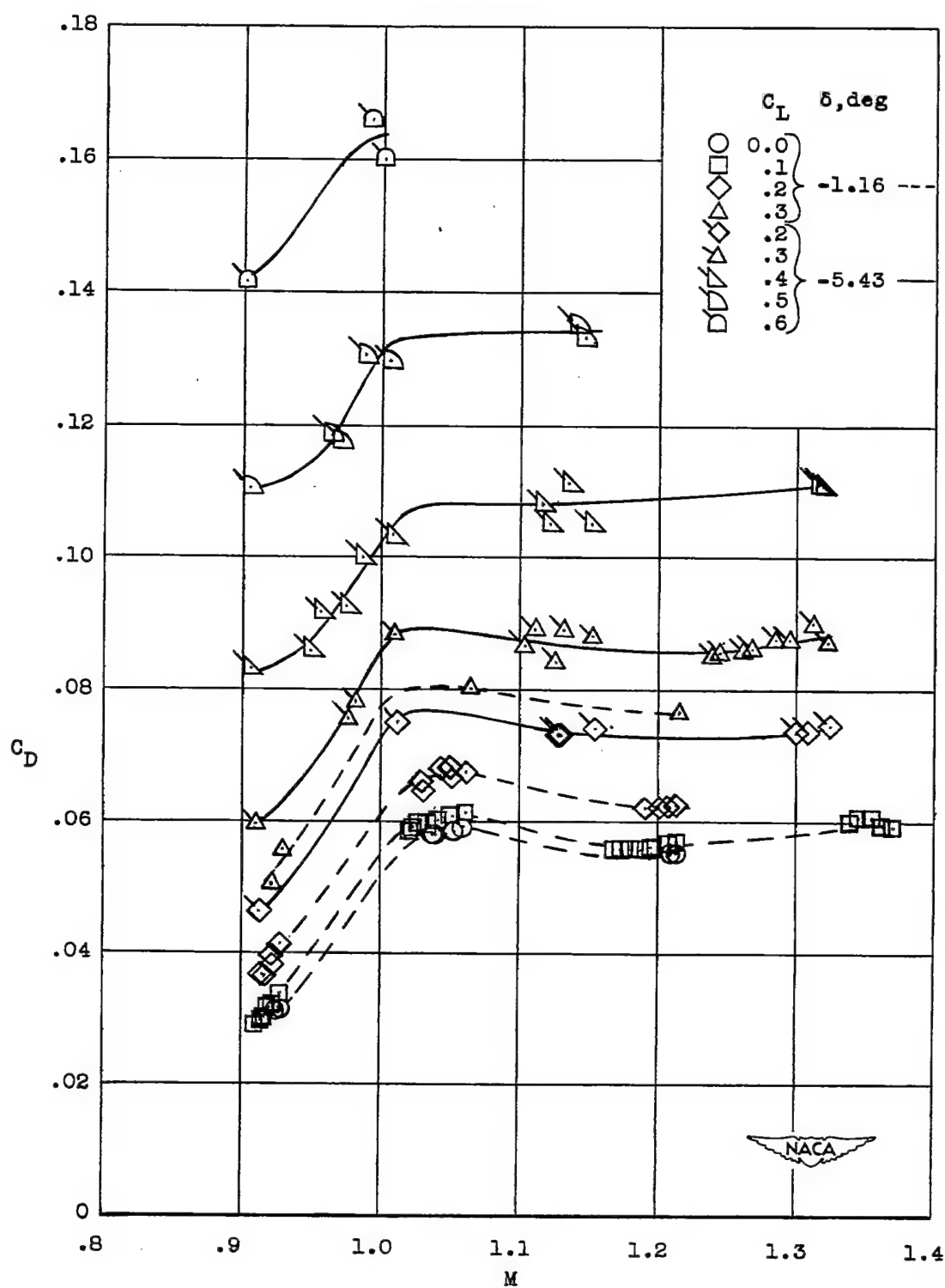
Figure 9.- Variation of drag coefficient with Mach number and lift coefficient.
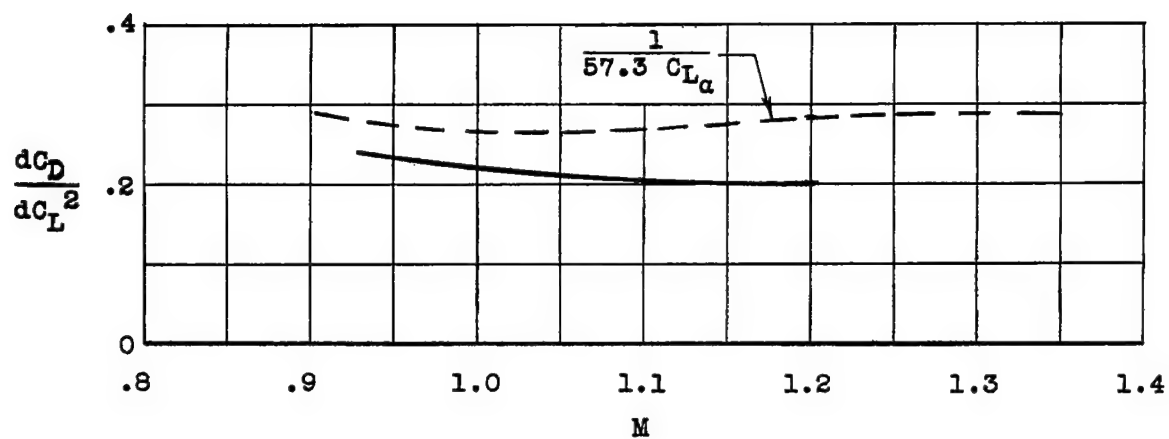
(a) $\delta = -1.16°$.
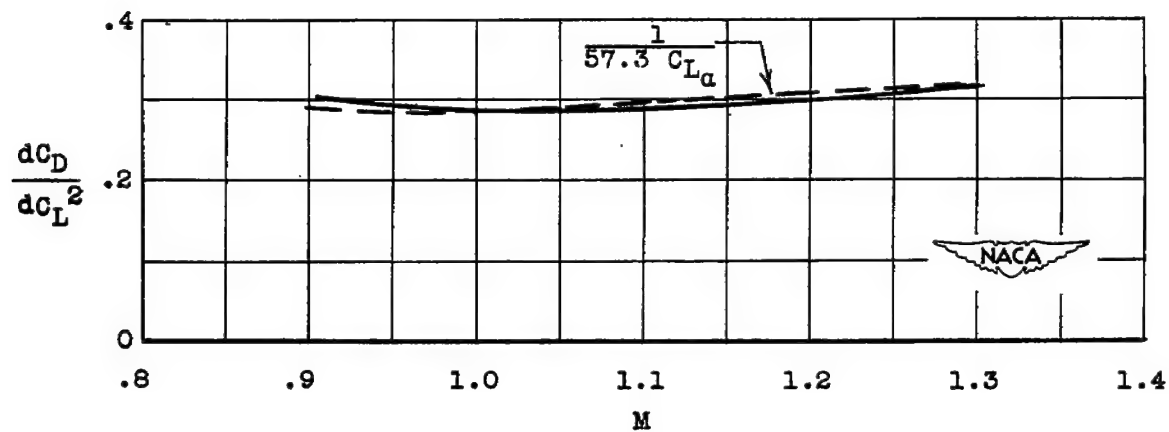
(b) $\delta = -5.43°$.

Figure 10.- Induced drag factor.

(a) δ = -5.43°.
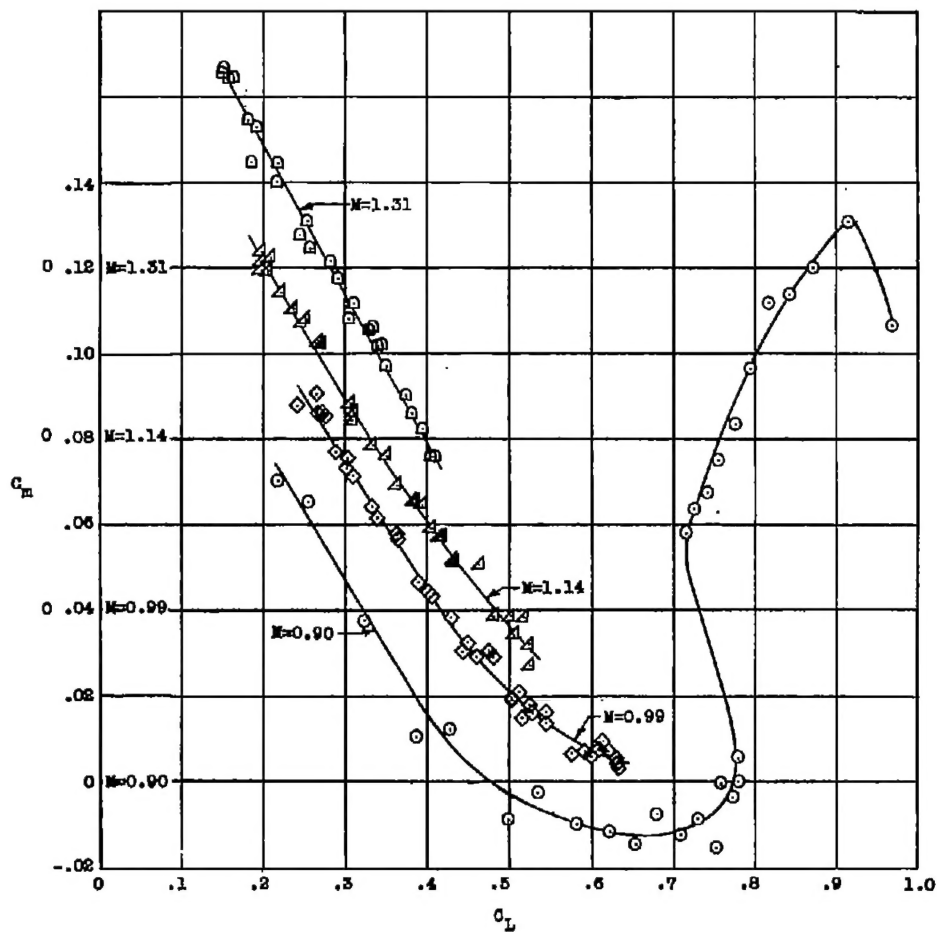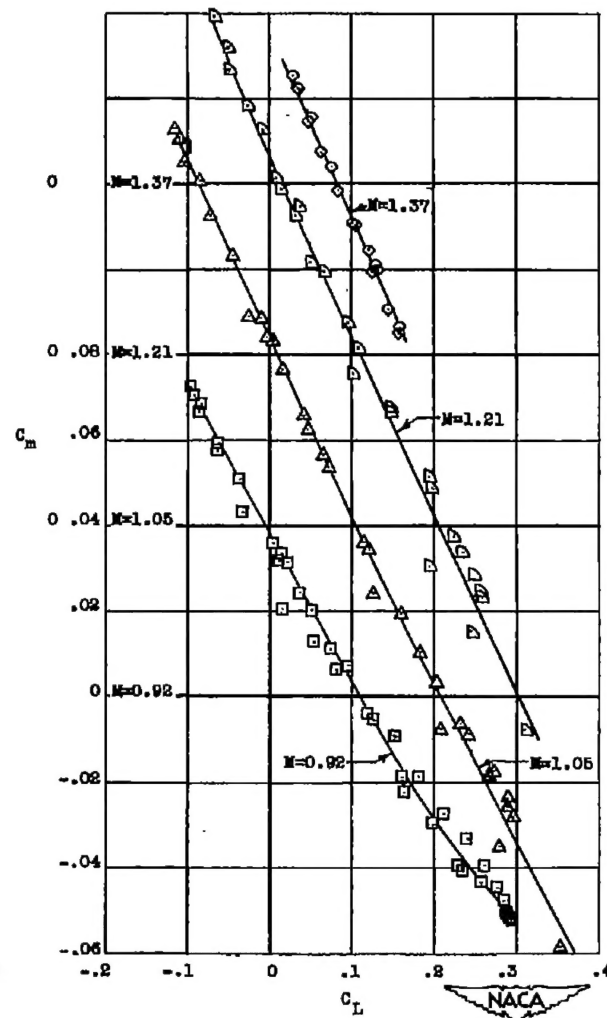
(b) δ = -1.16°.

Figure 11.- Variation of pitching-moment coefficient with lift coefficient.
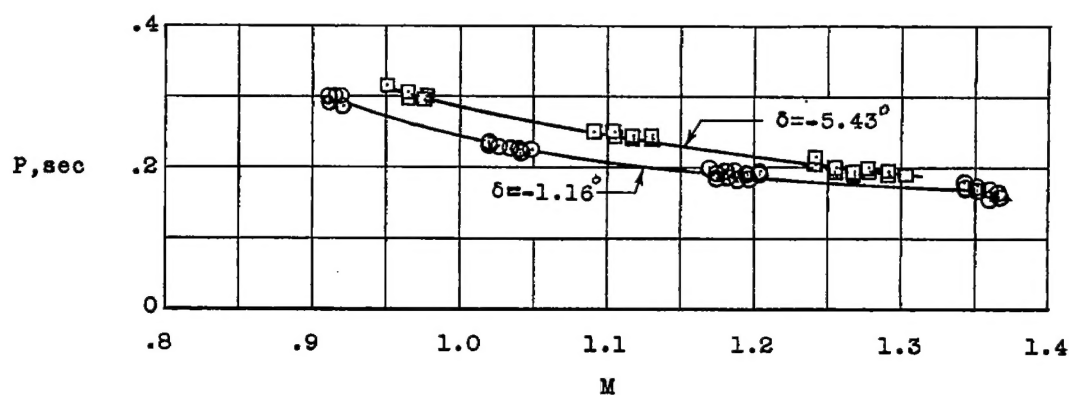
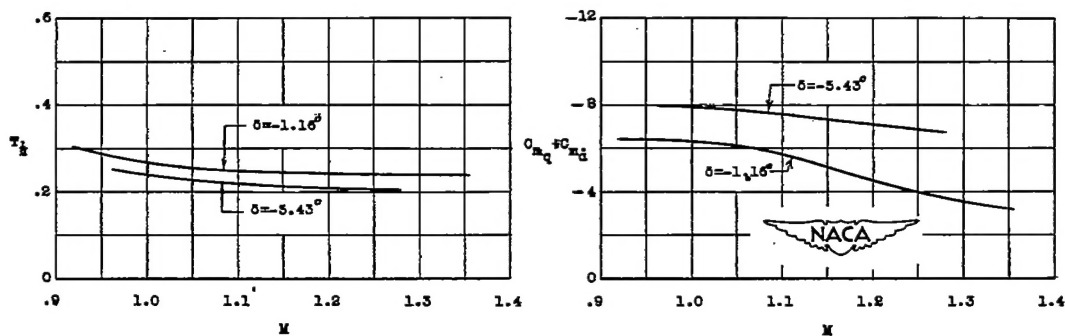(a) Period of pitch oscillation.
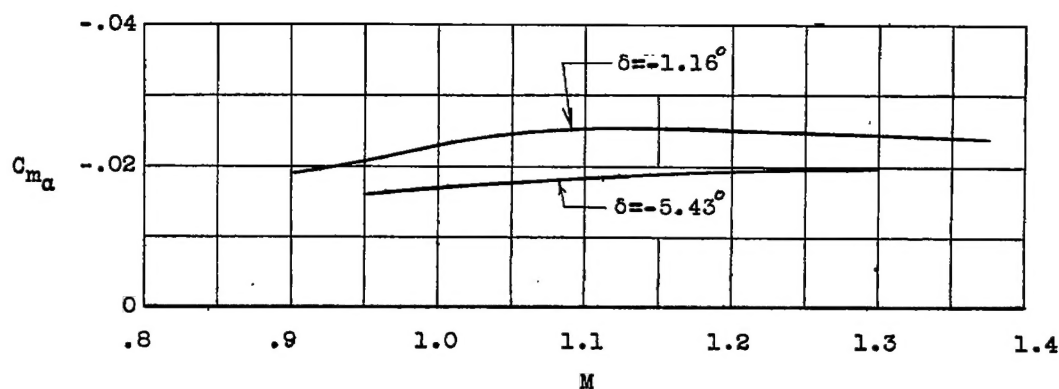
(b) Longitudinal stability parameter C_{m_α}.
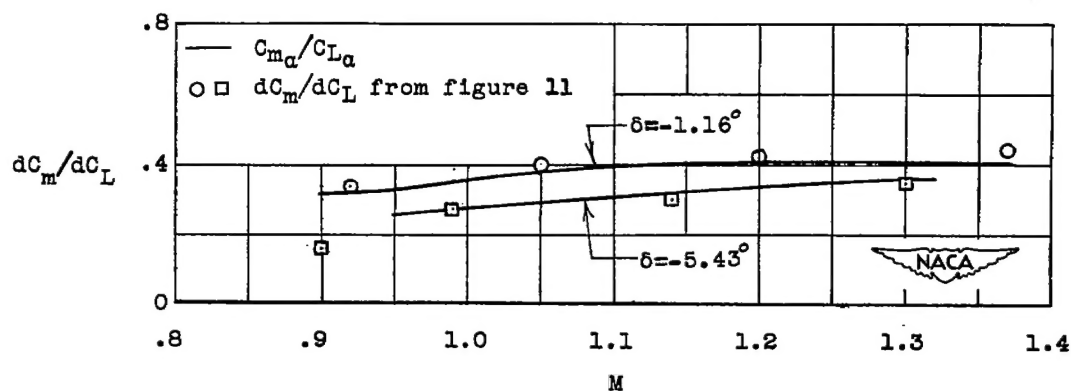
(c) Longitudinal stability parameter dC_m/dC_L.

Figure 12.- Static longitudinal characteristics with center of gravity
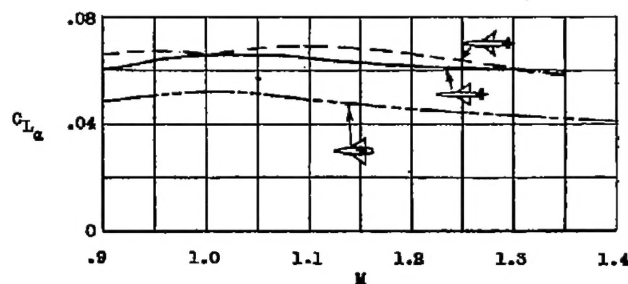   at 20.6 percent of the mean aerodynamic chord.

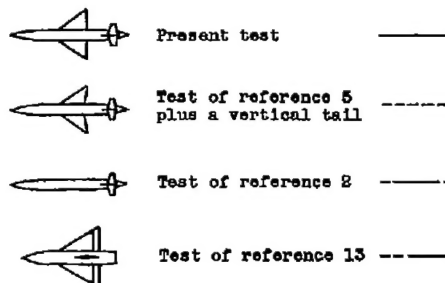|	Avg. M	δ, deg
□	0.92	-1.16
◇	.98	-5.43
△	1.04	-1.16
◁	1.12	-5.43
◁	1.19	-1.16
◁	1.29	-5.43
◇	1.36	-1.16
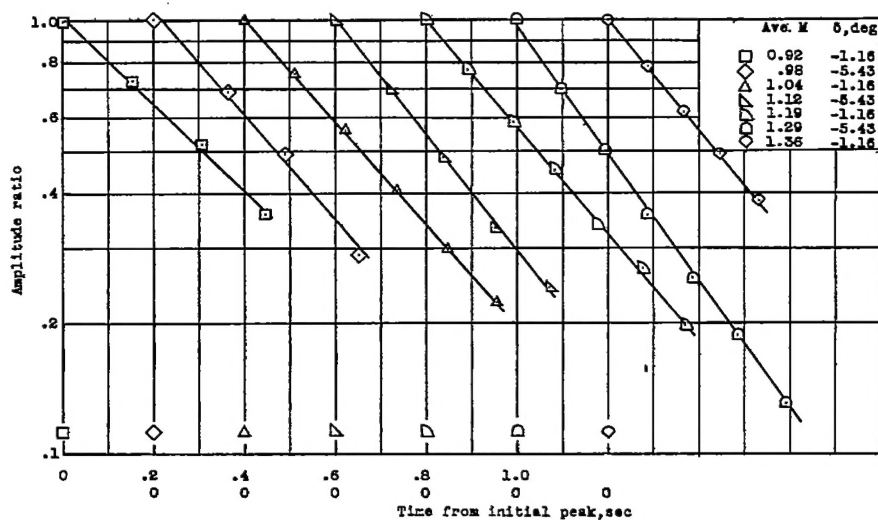
(a)   Variation of amplitude ratio with time.
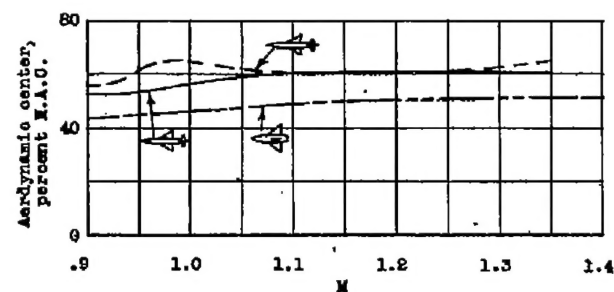

(b) Time to damp to
one-half amplitude.

(c)   Rotary-damping coefficient.

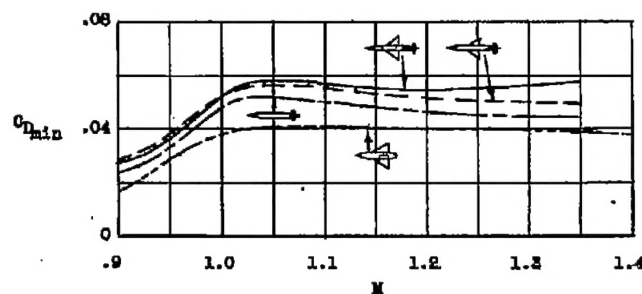Figure 13.- Damping-in-pitch characteristics.

Present test ————

Test of reference 5
plus a vertical tail ———·—

Test of reference 2 ———
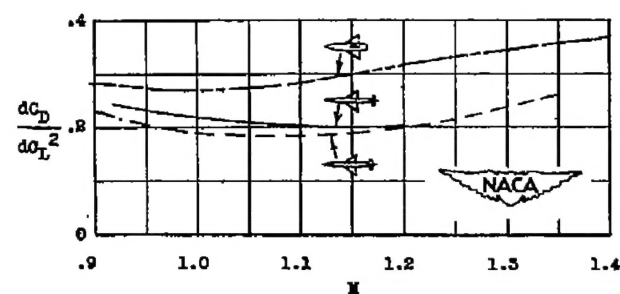
Test of reference 13 ——·——

(a) Lift-curve slope.

(c) Aerodynamic-center location.

(b) Minimum drag coefficient.

(d) Induced drag factor.

Figure 14.- Comparisons of low-lift data ($\delta = -1.16^{\circ}$) with data of other
tests.